Energy and AI 12 (2023) 100225

Contents lists available at ScienceDirect

Energy and AI

journal homepage: www.sciencedirect.com/journal/energy-and-ai

Segmented thermoelectric generator modelling and optimization using artificial neural networks by iterative training

Yuxiao Zhu [a], Daniel W. Newbrook [a], Peng Dai [a], Jian Liu [b], C.H.Kees de Groot [a], Ruomeng Huang [a,*]

[a] School of Electronics and Computer Science, University of Southampton, Southampton, United Kingdom
[b] School of Physics, Shandong University, Shandong, China

HIGHLIGHTS

- Forward modelling of segmented TEG *via* iterative training artificial neural network.
- Factors including geometrical parameters, operating conditions, and contact resistance are considered.
- Prediction of TEG power density with extremely high accuracy over 98% using iterative training method compared to 94% using the traditional training method.
- Capability to perform TEG design optimization with much higher efficiency than the conventional approach.

GRAPHICAL ABSTRACT

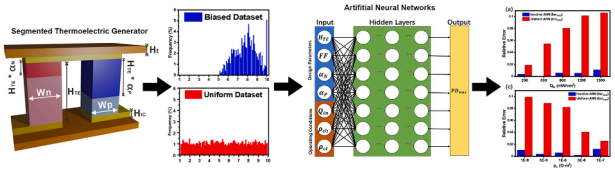

ARTICLE INFO

Keywords:
Segmented thermoelectric generator
Artificial neural network
Genetic algorithm
Optimization
Iterative training

ABSTRACT

Renewable energy technologies are central to emissions reduction and essential to achieve net-zero emission. Segmented thermoelectric generators (STEG) facilitate more efficient thermal energy recovery over a large temperature gradient. However, the additional design complexity has introduced challenges in the modelling and optimization of its performance. In this work, an artificial neural network (ANN) has been applied to build accurate and fast forward modelling of the STEG. More importantly, we adopt an iterative method in the ANN training process to improve accuracy without increasing the dataset size. This approach strengthens the proportion of the high-power performance in the STEG training dataset. Without increasing the size of the training dataset, the relative prediction error over high-power STEG designs decreases from 0.06 to 0.02, representing a threefold improvement. Coupling with a genetic algorithm, the trained artificial neural networks can perform design optimization within 10 s for each operating condition. It is over 5,000 times faster than the optimization performed by the conventional finite element method. Such an accurate and fast modeller also allows mapping of the STEG power against different parameters. The modelling approach demonstrated in this work indicates its future application in designing and optimizing complex energy harvesting technologies.

* Corresponding author.
E-mail address: r.huang@soton.ac.uk (R. Huang).

https://doi.org/10.1016/j.egyai.2022.100225

Available online 20 December 2022

Nomenclature

A_{TEG}	Top ceramic area of STEG (cm^2)
Q_{in}/A	Heat flux density (mW/cm^2)
H_t	Height of the ceramic layer
T_c	Cold-side temperature (K)
ρ_{ct}	Top Contact resistivity ($\Omega \cdot m^2$)
FF	Filling Factor
α_N	The ratio of N-type high-temperature material height to the overall STEG leg height
S	Seebeck coefficient
σ	Electrical Conductivity (S/m)
H_{TE}	Height of the STEG leg (mm)
H_{IC}	Height of the interconnect (mm)
W_n	Widths of the n-type leg (mm)
W_p	Widths of the p-type leg (mm)
ρ_{cb}	Bottom Contact resistivity ($\Omega \cdot m^2$)
PD_{max}	Power density (mW/cm^2)
α_P	The ratio of P-type high-temperature material height to the overall STEG leg height
k	Thermal Conductivity (W/m·K)
R^2	Coefficient of determination value

1. Introduction

Innovation in renewable technology needs to play a significant role in the roadmap toward net-zero emission (NZE) by 2050 [1]. Developing novel renewable energy technologies is key to staying on the path to NZE. Thermoelectric generators (TEGs) can convert thermal wasted energy into electricity and have also attracted tremendous attention as a potential renewable energy technology [2]. TEGs are based on the Seebeck effect. A voltage will be generated when a temperature gradient is applied across a thermoelectric material. By placing the n-type and p-type thermoelectric materials thermally in parallel and electrically in series, power can be generated under a solid-state operation mode with high reliability, low maintenance requirement, and long lifetime [3, 4]. Despite those advantages, TEGs suffer less efficiency than their counterpart technologies (e.g., solar cells), which significantly limits their large-scale application. Such low efficiency originates from the limited material thermoelectric properties and preliminary generator design and optimization [5]. Over the past few decades, significant breakthroughs have been made to enhance thermoelectric materials' performance (evaluated by the figure-of-merit, ZT). With prominent examples includes SnSe [6], PbTe [7], Zn_4Sb_3[8] for mid-high temperature applications and $Bi_2Te_{2.7}Se_{0.3}$ [9], $Bi_{0.4}Sb_{1.59}Ge_{0.01}Te_3$ [10] and $Mg_3Sb_{1.5}Bi_{0.5}$ [11] for room-temperature applications been reported to reach high ZT values over 1.

Concurrently with the development of thermoelectric materials, novel TEG modules have also been proposed to improve their power generation performance [5]. Segmented TEG (STEG) is a critical module concept proposed to improve efficiency when operating under a significant temperature difference [12]. STEG combines a highly efficient material at high temperatures with another highly efficient material at low temperatures. Under ideal conditions, the two materials will operate only in their most efficient temperature range, thereby improving overall performance [13]. Flueiral et al. proposed a new STEG design which achieved a conversion efficiency of 15% under a temperature difference of 675 K, 20% higher than previously achieved [14]. As ZT is a highly temperature-dependant parameter and each thermoelectric material usually has its optimum performance over a relatively small temperature range, the development of STEG that combines two or more materials with different operating temperatures in series in the TEG legs has been proven to be an effective way to improve the TEG efficiency [15]. In particular, Zhang et al. have demonstrated a record-high efficiency of up to 12% by deploying STEG modules consisting of Bi_2Te_3--based alloys and $CoSb_3$-based filled skutterudites [16].

With the high-performance material and TEG module developed, the next task is to optimize the module design for higher efficiency. However, optimizing the TEG module is challenging due to the temperature dependence of the material properties and the inherent complexity in TEG designs involving several inter-dependant parameters [17]. Several optimization approaches, including genetic algorithms that simulate natural selection[18, 19], the Taguchi method [20], and the Hill-climbing algorithm [21], have been proposed. Nevertheless, TEG design optimization requires rigorous procedures and accurate TEG modelling approaches. In general, the modelling of TEGs can be conducted through a theoretical system or numerical process. Simple theoretical models have been developed to investigate the optimization of thin-film TEGs [22]. Snyder et al. discussed the relationship between TEG efficiency and materials through theoretical modelling [23]. Fan has also modelled STEG under certain conditions through theoretical equations [24]. Another approach for predicting TEG performance is to use numerical modelling. The primary approach to numerical modelling is to solve the physical equations to calculate the required parameters. The established equations can be divided into one-dimensional models and three-dimensional models. Many researchers have proposed simplifying the three-dimensional model into a one-dimensional one to simplify the computational difficulties. Parameters such as the current and voltage of the TEG are estimated by integration in a single dimension, simplifying the calculation [25, 26]. Zhang et al. developed a one-dimensional model to discuss the relationship between leg ratio and the efficiency of segmented TEGs [23]. Zhu et al. combined a one-dimensional (1-D) numerical model of the STEG with a genetic algorithm for optimization [18]. Despite their high modelling speed, these simplified 1-D models ignored the lateral thermoelectric effects and boundary conditions due to the limitation of their models. This limitation inevitably leads to lower modelling accuracy when comparing with 3-dimensional (3-D) numerical models. [27]. The 3-D models based on commercial finite element method (FEM) software such as ANSYS and COMSOL allow the consideration of all thermoelectric parameters and boundary conditions and enables high modelling accuracy. Ouyang et al. modelled the STEG through ANSYS [28], and Ge et al. applied a 3-D COMSOL model in their evolutionary algorithm-based optimization of a STEG [29]. However, this accuracy is achieved in exchange for significant calculation resources and computing time.

Artificial neural networks (ANNs), the basis of deep learning technology, have recently attracted tremendous attention for their application in extensive data analysis [30], image recognition [31], and modelling [32]. Owing to its powerful fitting ability, the regression ANN models have also been utilized in the energy sector by modelling energy consumption [33] and forecasting energy demand [34, 35]. Recently, we have applied ANN in the forward modelling of a conventional TEG [36]. The ANN model can intelligently learn the non-linear relations. In this work, it is between the TEG inputs (i.e., geometrical parameters and operating conditions) and its performance (i.e., power density and efficiency) [37]. Research on artificial neural networks for thermoelectric generators has also included collecting data from experimental data to train the network and make predictions [38]. Garud et al. modelled the thermoelectric generators with an artificial neural network and the Adaptive Neuro-Fuzzy Interface System to predict the results [39]. In addition, Angeline et al. predicted the performance of hybrid thermoelectric generators by artificial neural networks [40]. Also, Wang et al. added the selection of thermoelectric materials to the artificial neural network modelling [41]. Compared with theoretical and numerical approaches, ANN is much more cost-effective and capable of balancing accuracy and speed. It can also be coupled with a genetic algorithm to realize fast TEG design optimization. However, most of the ANN models are based on the standard bulk TEG with only one TE material for each leg. A more complex Segmented TEG is modelled in our article which

contains two TE materials for each leg in order to maximise the efficiency. However, this introduces complexity in the modelling as one will need to consider additional parameters such as material ratios for each leg. In addition, a larger operating range (e.g. heat influx, temperature difference) needs to be considered to appreciate the advantage of STEG.

As a data-driven approach, the performance of ANN crucially depends on both the quantity and quality of the training dataset, which is traditionally generated *via* a randomized procedure. The network learns to interpolate the training data through gradient descent during the training process. However, such interpolation can be unsatisfactory. It sometimes happens when the training data has sharp features, or the network aims to model some specific features [42]. In the case of TEG modelling, we are particularly interested in TEG designs that could produce high power performance. However, such designs only constitute a small fraction of the training dataset. For the ANN to accurately predict these high-performance designs, the dataset size needs to be sufficiently large, especially for complex designs that involve multiple parameters. A large dataset is essential for STEG due to the complexity introduced by additional TE materials and parameters in the design [43]. Nevertheless, a large dataset implies high demand for a computational resource if the dataset is generated by numerical simulations (e.g., FEM), which can be prohibitive for the application of ANN. It is, therefore, essential to develop a training approach that allows high modelling accuracy for high-power performance STEG designs without additional requirements for the dataset size.

This work reports the forward modelling of the STEG using a fully connected ANN. We aim to improve the modelling accuracy on high-power performance designs while keeping the same training dataset size. Consequently, we adopted a novel iterative training strategy to strengthen the proportion of these designs in the dataset through an optimization process [44, 45]. During the iterative training process, the ANN is initially trained through a random, uniformly distributed dataset. Based on this trained neural network, a new dataset is generated with an optimization algorithm (e.g., genetic algorithm) to contain high-power performance designs. This dataset is used to train a new neural network. After training, the ANN can predict the STEG power performance over 100,000 times faster than the equivalent FEM simulation (under the same computing environment). More importantly, the iteratively trained network demonstrate significantly improved performance when predicting high-performing STEG designs. This superior modelling capability in STEG analysis and design optimization by coupling with the genetic algorithm is also demonstrated. Under the same STEG optimization process, we demonstrate an improved prediction accuracy from 93.0% to 99.4% by adopting this iterative training method.

2. Method

2.1. Physical model and boundary conditions

Fig.1a shows the STEG modelled in this work. The top and bottom brown insulating layers in Fig. 1a are aluminium nitride ceramics with high thermal conductivity. Immediately adjacent to the insulation is the top electrode made of copper. Each TEG leg consists of a high-temperature (top) and a low-temperature (bottom) thermoelectric material. Thermoelectric materials developed from past studies are selected. Their associated *ZT* values are shown in Fig 1b. For the n-type leg, $PbTe_{0.998}I_{0.002}$–3%Sb [46] was selected as the high-temperature material (dark red), and $Bi_2Te_{2.7}Se_{0.3}$ [9] was selected as low-temperature material (light red). For the p-type leg, $K_{0.02}Pb_{0.98}Te_{0.15}Se_{0.8}$ (dark blue) [47] and $Bi_{0.5}Sb_{1.5}Te_3$ (light blue) [48] were selected as high and low temperature materials, respectively. The temperature-dependant thermoelectric properties, including the Seebeck coefficient (S), and electrical and thermal conductivities (σ and k), are shown in Fig. S1. The fitting equations for each property are listed in Table S1.

The model variables are divided into design parameters and operating conditions. Design parameters include the geometrical height (H_{TE}) and width (W_{TE}) of the n-type and p-type legs. In this work, the widths of the two legs are kept the same and can be defined by the fill factor (FF), which is the ratio between the cross-sectional areas of the two legs ($W_n^2 + W_p^2$) and the entire device (A_{TEG}). For STEG, two additional design parameters, α_N and α_P, need to be defined to model the ratio of the n-type and p-type high-temperature material height to the overall leg height (H_{TE}). The operating conditions involve the density of heat flux into the thermoelectric generator (Q_{in}) as well as the electrical contact resistivities at the electrode and thermoelectric materials interface. It is worth mentioning that the STEG can also be modelled under the constant temerature difference conditions. However, only the constant heat flux conditions is considered in this work as such scenario is more common in the real world. Electrical contact resistivities between the upper and lower electrode to material interfaces (ρ_{ct} and ρ_{cb}) are also included in the model as the operating conditions. In addition, several parameters are kept constant in the model. The insulation thickness (H_t) and the electrode thickness (H_{IC}) are both fixed at 0.5 mm. The entire device area (A_{TEG}) is fixed at 1 cm^2 Moreover, only one thermocouple is investigated. In addition, the cold side temperature T_c is fixed at 293.15 K and convectional heat flux on all open internal surfaces with a heat transfer coefficient of 1 mW/(cm^2·K) and external temperature of 293.15 K to include surface heat convection to air [49].

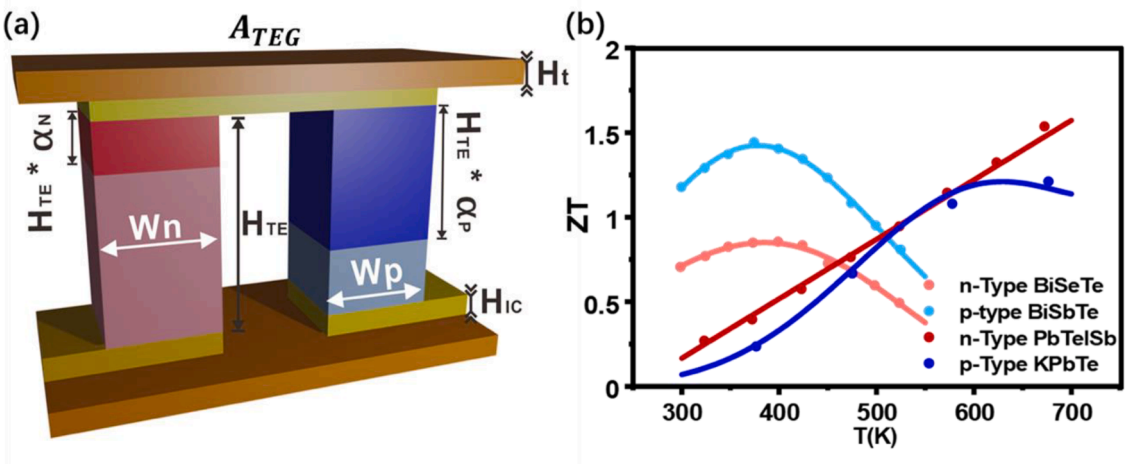

Fig. 1. (a) Schematic of the singe-pair segmented thermoelectric generator modelled in this study. Temperature-dependant. (b) the *ZT* of the n-type and p-type thermoelectric materials selected for the STEG in this work [9, 46–48].

2.2. Dataset generation and ANN training

3-D FEM-based simulations using COMSOL Multiphysics® software were used to generate the dataset for ANN training. This commercial simulation tool was chosen for its robust and accurate calculation of the parameters associated with the complex TEG model [50]. The specific parameter ranges and resolutions for all variables are tabulated in Table 1. In the STEG COMSOL modelling, the relevant governing equations are:

$$J = \sigma\left(-\nabla V + E_{emf}\right) \tag{1}$$

$$E_{emf} = -S\nabla T \tag{2}$$

$$q = PJ - k\nabla T \tag{3}$$

$$Q_{th} = -\mu_{th}\mathrm{J}\nabla T \tag{4}$$

$$P = ST \tag{5}$$

$$\rho C_p u\cdot\nabla T = \nabla\cdot(k\nabla T) + JE \tag{6}$$

where J is the current density, σ the electrical conductivity, V the voltage, S the Seebeck coefficient, T the temperature. Q_{th} is the heat generated by the Thomson effect, and μ_{th} is Thomson coefficient. P is Peltier coefficient. q and k are the heat flux and thermal conductivity, respectively. Eq. (6) describes electromagnetic heating, where ρ is the density, C_p is the heat capacity and u is the velocity field. The electrical terminal was connected directly to a load resistance for each simulation and swept from 1/100 to 100 times the estimated internal resistance. The maximum output power was then extracted from a parabolic fit of the output power against the current, as shown in Fig. S2. The impact of mesh size on the simulation accuracy was evaluated by simulating an identical parameter set with varying mesh sizes, as shown in Fig. S3. The "Fine" mesh size with 8012 elements has been employed for all simulations due to its high accuracy and reasonable computation time.

The dataset is generated uniformly and randomly based on the range and resolution of Table 1 as the input dataset of ANN (H_{TE}, FF, α_N, α_P, ρ_{ct}, ρ_{cb}, Q_{in}). The resulting dataset is therefore referred to as a uniform dataset. These variables were subsequently simulated in COMSOL Multiphysics® software to obtain the corresponding output maximum power density (PD_{max}) amongst different load resistors of the STEG as the output dataset of ANN. As the simulation focuses on constant heat flux, efficiency and power density can be calculated from each other. Therefore, only one parameter, power density (PD_{max}), was selected as output in the dataset.

The structure of the ANN in this work is shown in Fig. 2. The network contains an input layer that includes four design parameters (H_{TE}, FF, α_N, α_P) and three operating conditions (ρ_{ct}, ρ_{cb}, Q_{in}), as well as an output layer containing the STEG power performance (PD_{max}). There are five hidden layers between the input and output layers, with 200 neurons per layer. The network training begins by dividing the dataset into three sub-datasets for training, validation, and testing. Training data are fed to the ANN to optimize the network by updating the weights and bias of each neuron through backpropagation; validation data are used to examine the network, serving as a check of the training and an indicator for any overfitting or under-fitting behaviour during the training process; testing data are entirely new data to the network and were used to test the prediction accuracy of the network after training. The ANN is trained by taking the input dataset and computing it in the neural network to produce the ANN output. The mean squared error (MSE), a standard loss function used in ANN training, is used to measure the difference between the ANN's computational output and the dataset's output. The MSE is reduced by adapting the ANN parameters. All network training was conducted through the Python platform using the PyTorch module. The specific training parameters and details of the training process can be found in the support information. All COMSOL simulation and python scripts are running on the platform of Intel 10980xe CPU with Radeon RX 6900XT graphic card.

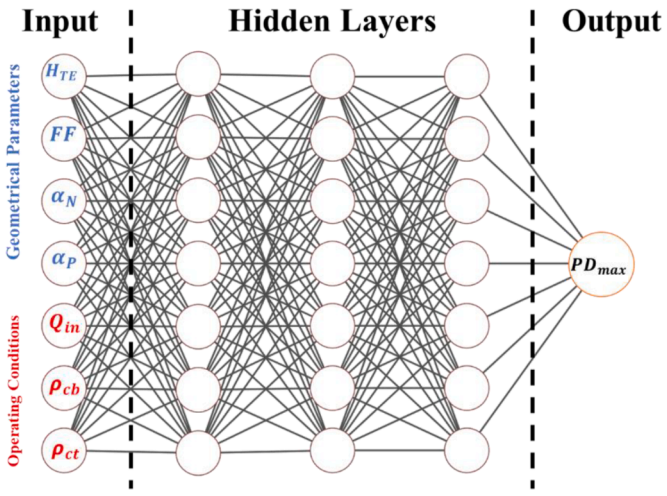

Fig. 2. . The architecture of the forward modelling ANN for predicting the power density of the STEG model. The input layer contains design parameters (H_{TE}, FF, α_N, α_P) and operating conditions (ρ_{ct}, ρ_{cb}, Q_{in}). The output layer contains power performance values (PD_{max}).

Table 1
Ranges and resolutions of the geometrical parameters and operating conditions used in this work.

Geometrical Parameter	Value Range	Resolution
Height of the TE leg (H_{TE})	**1–10 *mm***	**0.1 *mm***
Filling Factor (FF)	**0.05–0.95**	**0.01**
High-Temperature n-type TE leg height ratio (α_N)	**0.05–0.95**	**0.01**
High-Temperature n-type TE leg height ratio (α_P)	**0.05–0.95**	**0.01**
Operating Condition	**Value Range**	**Resolution**
Heat flux (Q_{in})	**100–2000 mW/cm^2**	**1 mW/cm^2**
Top side contact resistivity (ρ_{ct})	**10^{-9}–10^{-7} $\Omega\cdot m^2$**	**10^{-9} $\Omega\cdot m^2$**
Bottom side contact resistivity (ρ_{cb})	**10^{-9}–10^{-7} $\Omega\cdot m^2$**	**10^{-9} $\Omega\cdot m^2$**

3. Results and discussion

3.1. Iterative ANN training

A conventional ANN training involves only one dataset and one step training process as shown in Fig. 3a. Because the dataset is randomly generated and only contains low-performing TEG designs, the trained ANN (Uni_{4000}) is only capable of predicting low-performing TEGs. Our novel iterative training process has two steps as shown in Fig. 3b. An ANN was first trained using a dataset containing 3000 uniformly distributed input data (Uni_{3000}). The uniform distribution of the input parameters of Uni_{3000} is presented in Fig. S4. The ANN training process details are similar to our previous work [36] and are provided in the Supporting Information. We then coupled Uni_{3000} with genetic algorithm (GA), a meta-heuristic optimization algorithm, to identify the high-performing STEG designs at different operating conditions. The process of the specific genetic algorithm and the relevant parameters can be found in the Supporting Information. The corresponding STEG designs with the best performances can be obtained by generating 1000 different operating conditions based on Table 1. However, the maximum power density values generated by the neural network (Uni_{3000}) are not accurate enough. This inaccuracy is especially significant in the high PD_{max} region because fewer high-performance samples in the uniform dataset can be used as the output for the dataset. Instead, the newly

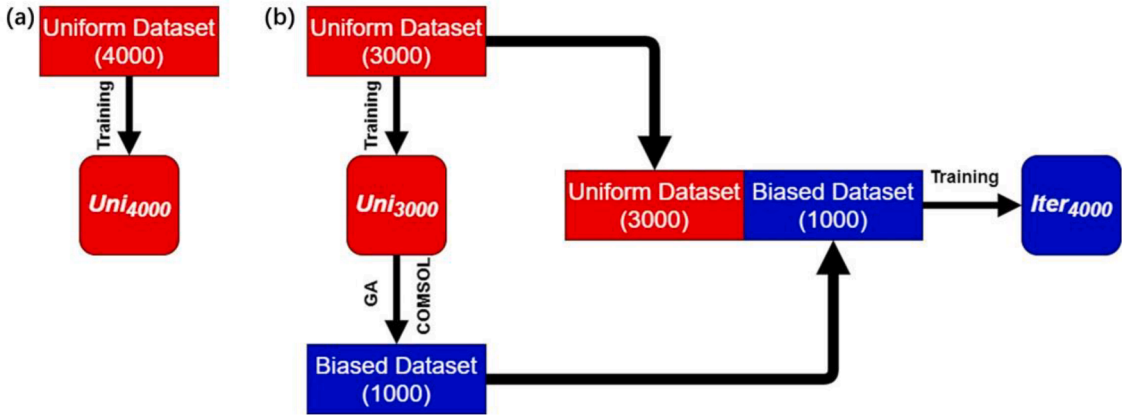

Fig. 3. (a) Coventional ANN training process. (b) Iterative ANN training process.

obtained design parameters and their operation conditions were simulated in COMSOL to produce the true maximum power density values. It is important to note that obtaining the Uni_{3000} network is essential in this iterative training process. It enables fast modelling of the STEG power performance, which significantly reduces the GA optimization time [36].

The dataset generated by the genetic algorithm was found to have unique characteristics. Fig. 4 compares the distribution of the GA generated dataset with the randomly generated dataset. The GA generated one is not conformed to a uniform distribution and is therefore referred to as the biased dataset. This highly non-uniform dataset represents STEG designs with high power performance. For example, the larger H_{TE} and smaller *FF* are favourable for achieving high power outputs (Fig. 4a and b). This trend is likely to be linked with the thermal conductance of the TE legs. Longer and smaller legs can result in a more significant temperature gradient across the TE materials under the constant heat flux condition. Similarly, both α_N and α_P also demonstrate biased distributions that correspond to the high-power STEG designs. The addition of such a biased dataset will help strengthen the proportion of these designs in the dataset.

After obtaining the biased dataset, a new dataset containing the original 3000 uniform data and this 1000 biased data was produced and used to train the new ANN (referred to as $Iter_{4000}$). To better evaluate the performance of this $Iter_{4000}$ network, a separate ANN was trained using a uniform dataset containing the same number of 4000 data (referred to as Uni_{4000}). The validation and test datasets in training two ANN were consistent during the training process. The specific training loss functions for $Iter_{4000}$ and Uni_{4000} are presented in Fig. S5.

3.2. Evaluation of two ANN training processes

We will first evaluate the prediction performance of the ANNs using a uniform test dataset. The uniform test dataset (U_{td}) was first randomly generated using 500 different input parameters (with operating

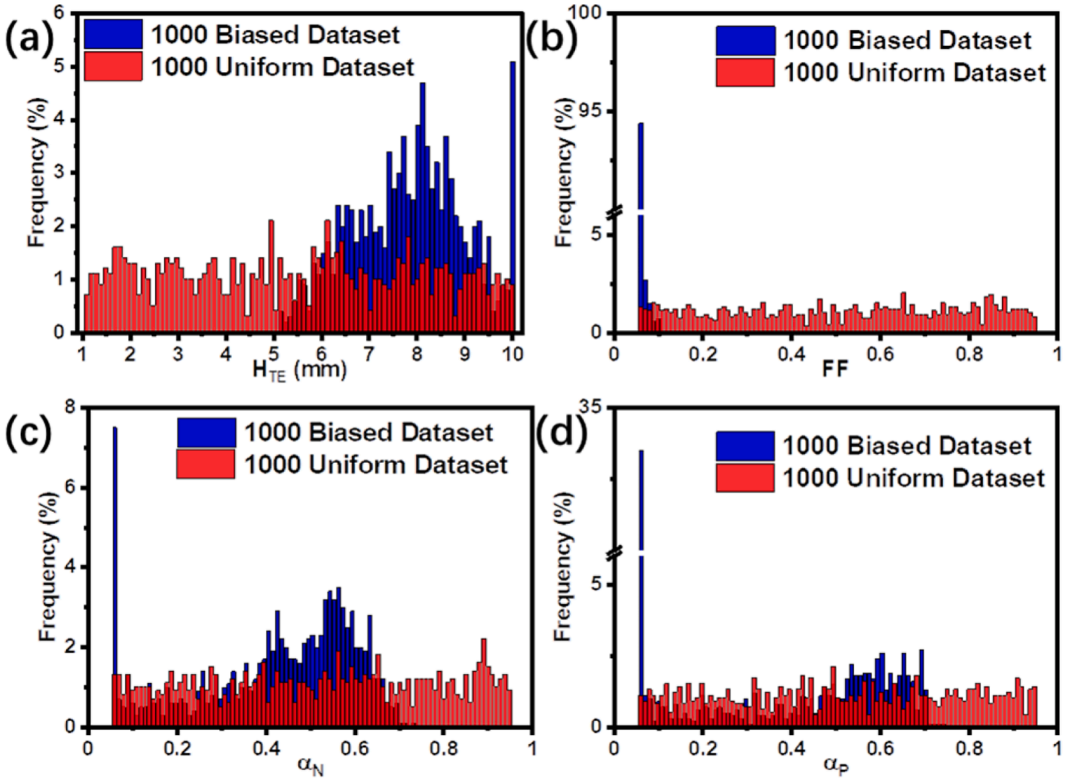

Fig. 4. Distribution of the design parameters (a) H_{TE}, (b) *FF*, (c) α_N, (d) α_P in the 1000 uniform datasets (red) and biased datasets (blue).

conditions and geometrical parameters). Then the input dataset is fed into COMSOL to simulate the output data. The distribution of U_{td} is shown in Fig. S8. We define the relative error for comparison to better demonstrate the prediction performance. The relative error is defined as:

Relative Error $= |P_{COMSOL} - P_{ANN}|/P_{COMSOL}$, where P_{COMSOL} is the true maximum power density obtained from COMSOL simulation while P_{ANN} is the results predicted by the ANN. On this basis, the prediction accuracy can be calculated as:

Prediction accuracy $= (1 - \textit{Relative Error}) \times 100\%$.

Fig. 5 presents the distribution and average relative error for the Uni_{4000} and $Iter_{4000}$ ANNs on the uniform test dataset. Both networks demonstrate minor relative errors of 0.021 and 0.024, corresponding to a high prediction accuracy of 97.9% for Uni_{4000} and 97.6% for $Iter_{4000}$. This accuracy is further confirmed by plotting the true PD_{max} (from simulation) in the uniform test set against the predicted PD_{max} by Uni_{4000} and $Iter_{4000}$, respectively (shown in Fig. 5b and c). It can be observed that the high prediction accuracy of our ANN prevails over the entire power range, producing a high coefficient of determination value (R^2) of over 0.999 for both networks. The slightly higher accuracy for Uni_{4000} can be explained by the difference between the additional 1000 uniform dataset and 1000 biased dataset used in their training process. Such a slight difference suggests that our $Iter_{4000}$ ANN can also provide accurate predictions for random STEG designs.

However, the critical advantage of iterative training lies in its prediction over biased high-performance STEG designs. To evaluate this performance, we generated a new biased test dataset with the aid of genetic algorithm optimization to measure the performance of ANN. We first generated 500 different sets of operating conditions randomly and fed them into GA and $Iter_{4000}$ to obtain the optimized geometrical parameters for each operating condition. These 500 input dataset were then simulated in COMSOL to achieve the true output and complete the dataset generation. This biased test dataset is named B_{td}. The distribution of B_{td} is presented in Fig. S8.

When such a biased test dataset was used for evaluation, the average relative error for Uni_{4000} ANN increased three times to 0.06, as shown in Fig 6a. This increase is accompanied by a large proportion of errors over 0.05, indicating that the ANN trained *via* the conventional approach has significant limitations in fitting the high-performance designs. On the other hand, the $Iter_{4000}$ ANN maintains its superior prediction performance with an average relative error of 0.02 and prediction accuracy of 98%. Fig. 6b and 6c present the true PD_{max} (from simulation) in the biased test dataset (B_{td}) against the predicted PD_{max}. It is also clear that a higher coefficient of determination value is obtained for the $Iter_{4000}$ ANN than the Uni_{4000} ANN. This improvement strongly suggests the benefit of the iterative training process. By including a proportion of biased data in the training dataset, the network excels in predicting high-performance STEG designs while retaining its high accuracy in random STEG design prediction.

We will now evaluate the prediction accuracy of the iterative ANN and the uniform ANN in STEG design optimization by coupling it with GA. GA optimization with COMSOL as the alternative forward modeller is conducted to obtain the genuinely optimized design and power performance as a reference. Fig. 7a presents the GA optimized PD_{max} under different heat flux conditions by coupling with COMSOL (black), Uni_{4000} (red), and $Iter_{4000}$ (blue). The optimized design parameters from each approach are listed in Table S4 and S5. It can be observed that the $Iter_{4000}$ optimized values are closer to the COMSOL optimized values than those optimized by Uni_{4000}. The relative errors of the two different ANNs (Uni_{4000}, $Iter_{4000}$) were calculated based on the optimal PD_{max} from the COMSOL simulation assisted GA optimization. Fig. 7b shows the relative errors of the optimized PD_{max} for the Uni_{4000} ANN (red bar) and $Iter_{4000}$ ANN (blue bar). The relative error for Uni_{4000} ANN increases significantly from 0.02 to over 0.1 when the input heat flux increases from 200 mW/cm^2 to 1500 mW/cm^2. Given that more considerable heat flux is more likely to produce a large PD_{max}, the poor performance of Uni_{4000} ANN is likely due to the limited high power performance data in the uniform training dataset. On the contrary, the relative error for $Iter_{4000}$ ANN is significantly smaller and remains below 0.02 for all heat flux conditions, suggesting a high accuracy over 98%. Similarly, it outperforms the Uni_{4000} ANN under various contact resistivity conditions, as shown in Fig. 7c and 7d. Over these 10 different operating conditions presented in Fig. 7, $Iter_{4000}$ achieved an average accuracy of 99.4% compared to the 93% accuracy obtained by Uni_{4000}, further suggesting the superiority of our iterative training process. In addition, the high accuracy for $Iter_{4000}$ also suggests it can sufficiently replace COMSOL simulation for STEG optimization. The average optimization time for ANN coupled GA is only ca. 6.3 s. In comparison, over 35,000 s (ca. 10 h) are required for COMSOL coupled GA under the same computational environment. This speed saves computational time and resources over 5000 times.

3.3. STEG analysis using iterative ANN

We have established the advantages of STEG modelling through iterative ANN, where its high prediction accuracy and speed ensure fast and accurate design optimization. Such benefits also allow the rapid generation of accurate parameter-performance data that are otherwise difficult to obtain through conventional modelling approaches. This large amount of data could contribute to the in-depth study of the STEG and unveil relations that have not been investigated before due to the complexity of the STEG structure. As an example, Fig. 8a presents the PD_{max} values as a function of H_{TE} and FF, where other parameters and conditions remain constant. The lines are the output of iterative ANN, and the triangles are the corresponding COMSOL simulation results. The PD_{max} increases progressively with increasing H_{TE} and decreasing FF, which could be understood as an increase of the TE leg thermal resistance and consequently resulting in a more considerable temperature difference across the device. The benefit of a more significant temperature difference outweighs the increased electrical resistance, which is likely dominated by contact resistance.

Fig. 8b demonstrates the dependence on different heat fluxes. As can be seen in Fig. 8b, the output PD_{max} increases as FF decreases when Q_{in} is

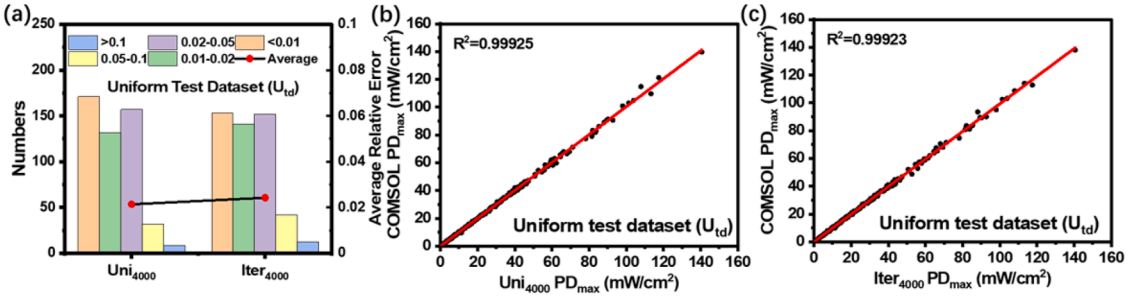

Fig. 5. Comparison of COMSOL output PD_{max} for two different ANNs on the uniform test dataset (U_{td}) (a) the histogram of the probability, (b) the average relative errors of Uni_{4000}, and (c)the average relative errors of $Iter_{4000}$.

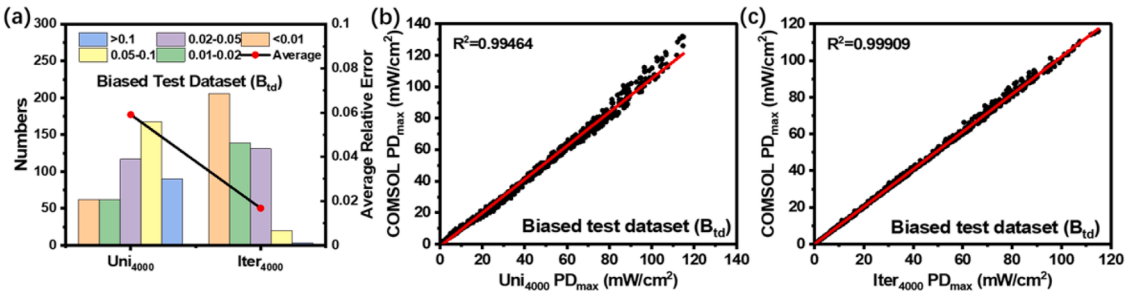

Fig. 6. Comparison of COMSOL output PD_{max} for two different ANNs on the biased test dataset (B_{td}) (a) the histogram of the probability, (b) the average relative errors of Uni_{4000}, and (c)the average relative errors of $Iter_{4000}$.

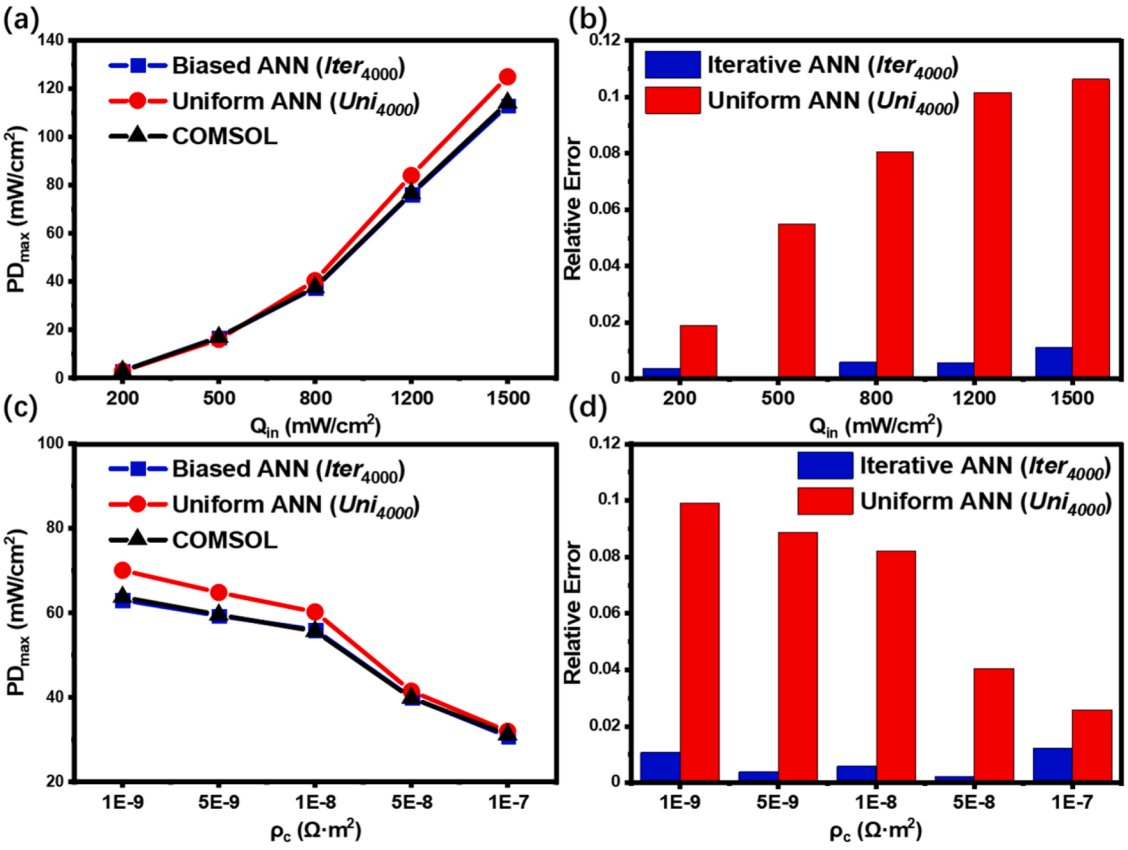

Fig. 7. Genetic algorithm optimized STEG PD_{max} using ANN $Iter_{4000}$ (blue), uniform ANN Uni_{4000} (red), and COMSOL simulation as forwarding modellers (a), and the associated relative errors from $Iter_{4000}$ (blue) and Uni_{4000} (red) compared with the COMSOL (b) as a function of different Q_{in}; Genetic algorithm optimized STEG PD_{max} using ANN $Iter_{4000}$ (blue), uniform ANN Uni_{4000} (red), and COMSOL simulation as forwarding modellers (c), and the associated relative errors from $Iter_{4000}$ (blue) and Uni_{4000} (red) compared with the COMSOL (d) as a function of different ρ_c.

relatively small. This tendency is because the temperature difference between the two ends of the STEG is not very significant. Hence, the benefit of the increase in thermal resistance outweighs the loss due to the rise in resistance. When $Q_{in} = 2000\ mW/cm^2$, on the other hand, the output increases and then decreases with decreasing *FF*. Since the energy from Q_{in} is so great that the temperature difference between the two ends of the STEG reaches the optimum operating region for high-temperature materials when the *FF* is reduced to around 0.1. The thermal resistance increase caused by continuing to minimise *FF* does not exceed the losses caused by the electrical resistance at this point, so the output PD_{max} is decreased. The triangles in Fig. 8 represent the COMSOL simulation results, which indicates that the values predicted by the $Iter_{4000}$ are very close to the real data and further validate the accuracy of the $Iter_{4000}$ model.

The relationships between the design parameters are complex when multiple parameters (e.g., α_N and α_P) vary simultaneously. Taking advantage of the ultra-fast computing speed, we performed a thorough mapping of PD_{max} under different α_N and α_P combinations as an example. Fig. 9 shows the PD_{max} of the biased ANN obtained by scanning α_N and α_P. Fig. 9a to 9c present the predicted PD_{max} mapping under the heat flux of 500, 1000, and 1500 mW/cm^2, respectively. It can be observed that when the Q_{in} is increased, the peak PD_{max} will be shifted to a larger α_N and α_P value to include more high-temperature material in the STEG design. Similarly, under different contact resistivity conditions, the impact of α_N and α_P values on PD_{max} is somewhat similar, as shown in Fig. 9d to 9f. However, as the contact resistance increases, the output power decreases significantly. Our iterative ANN can also effortlessly generate similar mappings over other design parameters and operating conditions.

Each mapping contains 8281 (91 × 91) modelling results and could

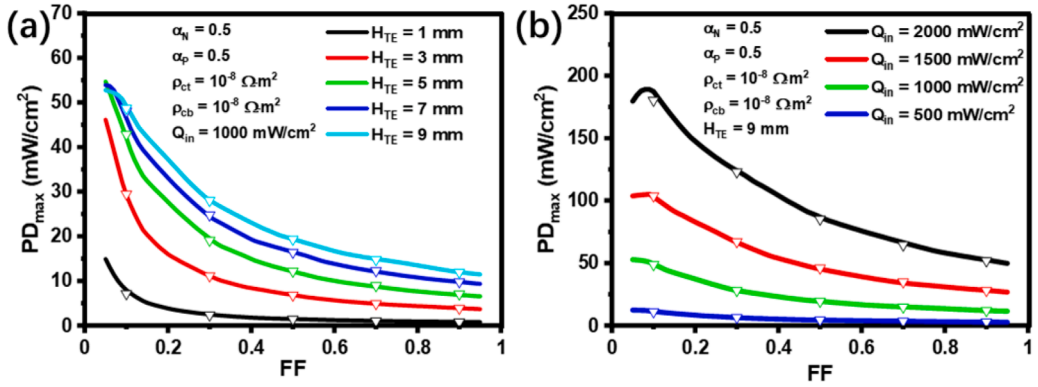

Fig. 8. PD_{max} obtained from iterative ANN (line) and COMSOL simulation (triangles) as a function of (a) H_{TE} and FF, (b) Q_{in}, and FF. .

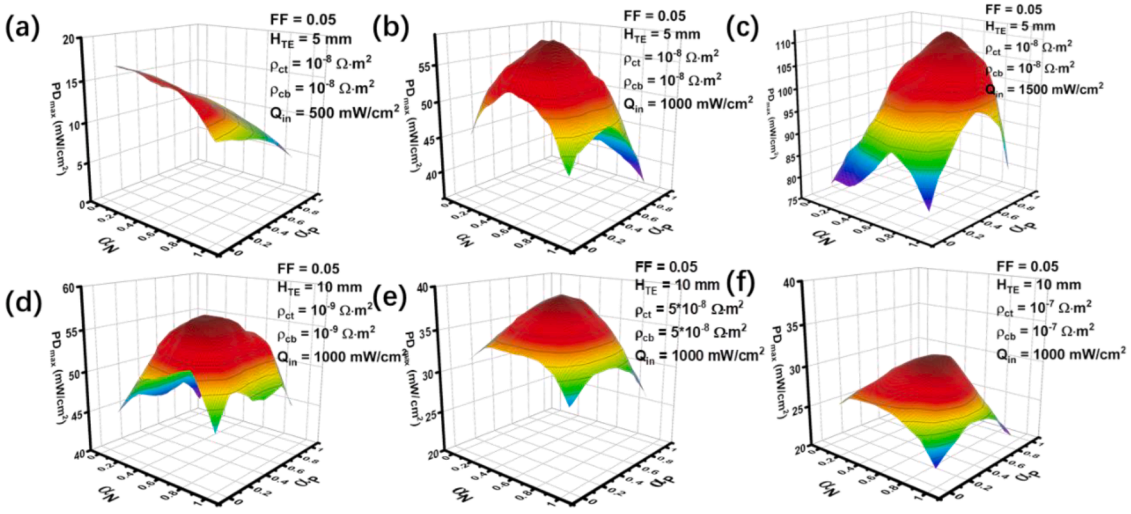

Fig. 9. PD_{max} of iterative ANN obtained by scanning α_N and α_P at different heat flux (Q_{in}) conditions of (a) 500 mW/cm^2, (b) 500 mW/cm^2, (c) 500 mW $/cm^2$, respectively with other parameters fixed; PD_{max} of iterative ANN obtained by scanning α_N and α_P at different electrical conductivity ($\rho_{ct} = \rho_{cb} = 10^{-9}$) conditions (d) $10^{-9}\Omega{\cdot}m^2$(e) 5 $\times$ $10^{-8}\Omega{\cdot}m^2$ and (f) $10^{-7}\Omega{\cdot}m^2$, respectively.

take over 330,000 s (~ 91 h) for COMSOL to simulate. The application of our iterative ANN will only take 3 s under the same computational environment, which represents over 100,000 times efficiency improvement. Even adding the dataset preparation time it is also 2 times faster than COMSOL simulation. Moreover, this advantage will increase with more frequent use of the ANN. Fig. 10 shows the time required for both methods to perform multiple number of modelling and GA optimisations under the same computation conditions. The training time of the ANN is considered in this comparison. It is clear that the amount of time saved by using ANN easily recovers the up-front computational time for the network when more than 4000 modelling is required (Fig. 10a) or more than 2 GA optimisations are needed (Fig. 10b). This manifests the extremely high computational efficiency of our ANN approach.

Table 2 lists a range of reported works on the modelling of STEG in comparison to this work. Our iteratively trained ANN can provide more operating conditions and parameters than those theoretical and 1-D

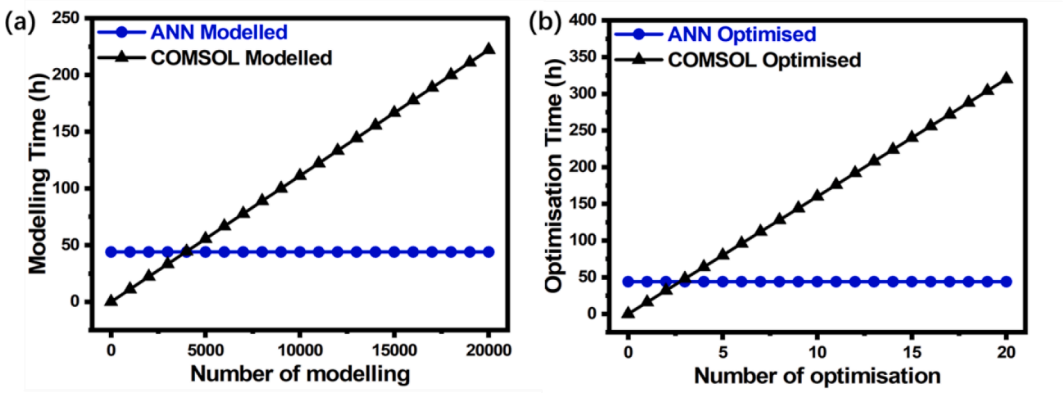

Fig. 10. The required computational time as a function of (a) the number of modelling and (b) the number of optimization for ANN (blue) and COMSOL (black).

Table 2
List of a literature review of STEG forward modelling methods.

Modelling Method	Coupling optimization algorithm	Temperature-dependant parameters	Electrical contact resistance	Non-linear effects in the horizontal direction	Convection	Ref
Numerical model (1-D)	**No**	**Yes**	**Yes**	**No**	**No**	[51]
Numerical model (1-D)	**Yes**	**Yes**	**Yes**	**No**	**Yes**	[18]
Numerical model (1-D)	**No**	**Yes**	**No**	**No**	**No**	[14]
Numerical model (1-D)	**Yes**	**No**	**No**	**No**	**No**	[52]
Numerical model (3-D)	**No**	**Yes**	**Yes**	**Yes**	**Yes**	[16]
Numerical model (3-D)	**No**	**Yes**	**Yes**	**Yes**	**No**	[28]
Numerical model (3-D)	**No**	**Yes**	**No**	**Yes**	**No**	[50]
Theoretical Model	**No**	**Yes**	**No**	**No**	**No**	[53]
Theoretical Model	**Yes**	**Yes**	**Yes**	**No**	**No**	[54]
Theoretical Model	**No**	**Yes**	**No**	**No**	**No**	[15]
Theoretical Model	**Yes**	**Yes**	**No**	**Yes**	**No**	[55]
ANN Model	**Yes**	**Yes**	**No**	**Yes**	**No**	[43]
This work	**Yes**	**Yes**	**Yes**	**Yes**	**Yes**	

numerical models. It also outperforms the 3-D numerical models with superior modelling speed.

4. Conclusions

In conclusion, this work uses an artificial neural network to report the forward power performance modelling for the segmented thermoelectric generator. After training using a dataset from 3-D COMSOL simulations, the neural network can predict the power performance under varying heat flux conditions from different design parameters. Moreover, it can still consider the electrical contact resistance, surface heat transfer, and other thermoelectric effects. An iterative training strategy was implemented to improve the prediction accuracy of the high-power performance STEG designs without increasing the training dataset size. This prediction accuracy of the iterative trained artificial neural network increases from 94% to over 98% without requiring a larger dataset. This high accuracy is essential to ensure the correct STEG design optimization results. In addition to superior accuracy, the neural network demonstrates extremely high efficiency, which is beneficial for fast design optimization and parameter dependence analysis. Coupled with a genetic algorithm, the network can achieve one design optimization for 6.3 s, 5000 times faster than COMSOL, but with almost identical optimized values. Large parameter scans have also revealed the relationship between the STEG power output and the segment material ratios. Only 3 s is required for the network to conduct a parametric scan containing 8281 data points, representing over 100,000 times of efficiency improvement. This machine learning enabled modelling approach demonstrated in this work indicates its future application in designing and optimizing complex energy harvesting technologies.

Appendix A. Supporting information

Supplementary data to this article can be found online at xxx.

Declaration of Competing Interest

The authors declare that they have no known competing financial interests or personal relationships that could have appeared to influence the work reported in this paper.

Data availability

All data supporting this study are available from the University of Southampton repository at DOI: https://doi.org/10.5258/SOTON/D2454

Acknowledgements

This work was supported by an EPSRC IAA funding. The authors acknowledge using the IRIDIS High-Performance Computing Facility and associated support services at the University of Southampton to complete this work. All data supporting this study are available from the University of Southampton repository at DOI: https://doi.org/10.5258/SOTON/D2454.

Supplementary materials

Supplementary material associated with this article can be found, in the online version, at doi:10.1016/j.egyai.2022.100225.

References

[1] IEA (2021), Global Energy Review 2021, https://www.iea.org/reports/global-energy-review-2021. Paris: 2021.
[2] Pourkiaei SM, Ahmadi MH, Sadeghzadeh M, Moosavi S, Pourfayaz F, Chen L, et al. Thermoelectric Cooler and Thermoelectric Generator Devices: A Review of Present and Potential Applications. Modeling and Materials. Energy 2019;186:115849. https://doi.org/10.1016/j.energy.2019.07.179.
[3] Snyder GJ, Toberer ES. Complex Thermoelectric Materials. Nat Mater 2008;7:105–14. https://doi.org/10.1038/nmat2090.
[4] Champier D. Thermoelectric generators: A Review of Applications. Energy Convers Manag 2017;140:167–81. https://doi.org/10.1016/j.enconman.2017.02.070.
[5] He R, Schierning G, Nielsch K. Thermoelectric Devices: A Review of Devices, Architectures, and Contact Optimization. Adv Mater Technol 2018;3:1700256. https://doi.org/10.1002/admt.201700256.
[6] Duong AT, Nguyen VQ, Duvjir G, Duong VT, Kwon S, Song JY, et al. Achieving ZT=2.2 with Bi-doped n-type SnSe single crystals. Nat Commun 2016;7:1–6. https://doi.org/10.1038/ncomms13713.
[7] Tan G, Shi F, Hao S, Zhao LD, Chi H, Zhang X, et al. Non-equilibrium Processing Leads to Record High Thermoelectric Figure of Merit in PbTe-SrTe. Nat Commun 2016;7:12167. https://doi.org/10.1038/ncomms12167.
[8] Caillat T, Fleurial JP, Borshchevsky A. Preparation and Thermoelectric Properties of Semiconducting Zn_4Sb3. J Phys Chem Solids 1997;58:1119.
[9] Yan X, Poudel B, Ma Y, Liu WS, Joshi G, Wang H, et al. Experimental Studies on Anisotropic Thermoelectric Properties and Structures of n-type $Bi_2Te_{2.7}Se_{0.3}$. Nano Lett 2010;10:3373–8. https://doi.org/10.1021/nl101156v.
[10] Wang YS, Huang LL, Zhu C, Zhang J, Li D, Xin HX, et al. Simultaneously Enhanced Power Factor and Phonon Scattering in $Bi_{0.4}Sb_{1.6}Te_3$ alloy doped with germanium. Scr Mater 2018;154:118–22. https://doi.org/10.1016/j.scriptamat.2018.05.026.
[11] Liu Z, Sato N, Gao W, Yubuta K, Kawamoto N, Mitome M, et al. Demonstration of Ultrahigh Thermoelectric Efficiency of ~7.3% in Mg_3Sb_2/MgAgSb Module for Low-temperature Energy Harvesting. Joule 2021;5:1196–208. https://doi.org/10.1016/j.joule.2021.03.017.

[12] Moore RG. Exact Computer Solution of Segmented Thermoelectric Devices. Adv Energy Convers 1962;2:183–95. https://doi.org/10.1016/0365-1789(62)90023-1.
[13] Snyder GJ. Application of the Compatibility Factor to the Design of Segmented and Cascaded Thermoelectric Generators. Appl Phys Lett 2004;84:2436–8. https://doi.org/10.1063/1.1689396.
[14] Caillat T, Fleurial J-P, Borshchevsky A. Development of High Efficiency Thermoelectric Generators using. Advanced Thermoelectric Materials 2008;1647:1647–51. https://doi.org/10.1063/1.54794.
[15] Tian H, Jiang N, Jia Q, Sun X, Shu G, Liang X. Comparison of Segmented and Traditional Thermoelectric Generator for Waste Heat Recovery of Diesel Engine. Energy Procedia 2015;75:590–6. https://doi.org/10.1016/j.egypro.2015.07.461.
[16] Zhang Q, Liao J, Tang Y, Gu M, Ming C, Qiu P, et al. Realizing a Thermoelectric Conversion Efficiency of 12% in Bismuth Telluride/Skutterudite Segmented Modules through Full-parameter Optimization and Energy-loss Minimized Integration. Energy Environ Sci 2017;10:956–63. https://doi.org/10.1039/c7ee00447h.
[17] Tian H, Sun X, Jia Q, Liang X, Shu G, Wang X. Comparison and Parameter Optimization of a Segmented Thermoelectric Generator by using the High Temperature Exhaust of a Diesel Engine. Energy 2015;84:121–30. https://doi.org/10.1016/j.energy.2015.02.063.
[18] Zhu L, Li H, Chen S, Tian X, Kang X, Jiang X, et al. Optimization Analysis of a Segmented Thermoelectric Generator Based on Genetic Algorithm. Renew Energy 2020;156:710–8. https://doi.org/10.1016/j.renene.2020.04.120.
[19] Lamba R, Kaushik SC, Tyagi SK. Geometric Optimization of Trapezoidal Thermoelectric Heat Pump Considering Contact Resistances through Genetic Algorithm. Int J Energy Res 2018;42:633–47. https://doi.org/10.1002/er.3845.
[20] Chen WH, Huang SR, Lin YL. Performance Analysis and Optimum Operation of a Thermoelectric Generator by Taguchi Method. Appl Energy 2015;158:44–54. https://doi.org/10.1016/j.apenergy.2015.08.025.
[21] He H, Wu Y, Liu W, Rong M, Fang Z, Tang X. Comprehensive Modeling for Geometric Optimization of a Thermoelectric Generator Module. Energy Convers Manag 2019;183:645–59. https://doi.org/10.1016/j.enconman.2018.12.087.
[22] Newbrook DW, Huang R, Richards SP, Sharma S, Reid G, Hector AL, et al. Mathematical Model and Optimization of a Thin-film Thermoelectric Generator. JPhys Energy 2020;2:014001. https://doi.org/10.1088/2515-7655/ab4242.
[23] Snyder GJ, Ursell TS. Thermoelectric efficiency and compatibility. Phys Rev Lett 2003;91:148301/1-148301/4. https://doi.org/10.1103/PhysRevLett.91.148301.
[24] Fan L, Zhang G, Wang R, Jiao K. A comprehensive and time-efficient model for determination of thermoelectric generator length and cross-section area. Energy Convers Manag 2016;122:85–94. https://doi.org/10.1016/j.enconman.2016.05.064.
[25] Suter C, Jovanovic ZR, Steinfeld A. A 1kW$_e$ Thermoelectric Stack for Geothermal Power Generation - Modeling and Geometrical Optimization. Appl Energy 2012;99:379–85. https://doi.org/10.1016/j.apenergy.2012.05.033.
[26] Shen ZG, Wu SY, Xiao L, Yin G. Theoretical Modeling of Thermoelectric Generator with Particular Emphasis on the Effect of Side Surface Heat Transfer. Energy 2016;95:367–79. https://doi.org/10.1016/j.energy.2015.12.005.
[27] Chen WH, Lin YX, Wang XD, Lin YL. A Comprehensive Analysis of the Performance of Thermoelectric Generators with Constant and Variable Properties. Appl Energy 2019;241:11–24. https://doi.org/10.1016/j.apenergy.2019.02.083.
[28] Ouyang Z, Li D. Modelling of Segmented High-performance Thermoelectric Generators with Effects of Thermal radiation, Electrical and Thermal Contact Resistances. Sci Rep 2016;6:1–12. https://doi.org/10.1038/srep24123.
[29] Ge Y, Liu Z, Sun H, Liu W. Optimal Design of a Segmented Thermoelectric Generator Based on Three-dimensional Numerical Simulation and Multi-objective Genetic Algorithm. Energy 2018;147:1060–9. https://doi.org/10.1016/j.energy.2018.01.099.
[30] Najafabadi MM, Villanustre F, Khoshgoftaar TM, Seliya N, Wald R, Muharemagic E. Deep Learning Applications and Challenges in Big Data Analytics. J Big Data 2015;2:1–21. https://doi.org/10.1186/s40537-014-0007-7.
[31] Voulodimos A, Doulamis N, Doulamis A, Protopapadakis E. Deep Learning for Computer Vision: A Brief Review. Comput Intell Neurosci 2018:2018. https://doi.org/10.1155/2018/7068349.
[32] Wei H, Bao H, Ruan X. Perspective: Predicting and optimizing thermal transport properties with machine learning methods. Energy AI 2022;8:100153. https://doi.org/10.1016/j.egyai.2022.100153.
[33] Kolb B, Lentz LC, Kolpak AM. Discovering charge density functionals and structure-property relationships with PROPhet: A general framework for coupling machine learning and first-principles methods. Sci Rep 2017;7:1–9. https://doi.org/10.1038/s41598-017-01251-z.
[34] Wang T, Zhang C, Snoussi H, Zhang G. Machine Learning Approaches for Thermoelectric Materials Research. Adv Funct Mater 2020;30:1–14. https://doi.org/10.1002/adfm.201906041.
[35] Wang ZL, Yokoyama Y, Onda T, Adachi Y, Chen ZC. Improved Thermoelectric Properties of Hot-Extruded Bi–Te–Se Bulk Materials with Cu Doping and Property Predictions via Machine Learning. Adv Electron Mater 2019;5. https://doi.org/10.1002/aelm.201900079.
[36] Zhu Y, Newbrook DW, Dai P, de Groot CHK, Huang R. Artificial Neural Network Enabled Accurate Geometrical Design and Optimisation of Thermoelectric Generator. Appl Energy 2022;305:117800. https://doi.org/10.1016/j.apenergy.2021.117800.
[37] Wang S-C. Artificial Neural Network. Interdiscip. Comput. Java Program. 2003:81–100. https://doi.org/10.1007/978-1-4615-0377-4_5.
[38] Ang ZYA, Woo WL, Mesbahi E. Artificial Neural Network Based Prediction of Energy Generation from Thermoelectric Generator with Environmental Parameters. J Clean Energy Technol 2017;5:458–63. https://doi.org/10.18178/jocet.2017.5.6.416.
[39] Garud KS, Seo JH, Cho CP, Lee MY. Artificial neural network and adaptive neuro-fuzzy interface system modelling to predict thermal performances of thermoelectric generator for waste heat recovery. Symmetry (Basel) 2020;12. https://doi.org/10.3390/sym12020259.
[40] Angeline AA, Asirvatham LG, Hemanth DJ, Jayakumar J, Wongwises S. Performance prediction of hybrid thermoelectric generator with high accuracy using artificial neural networks. Sustain Energy Technol Assessments 2019;33:53–60. https://doi.org/10.1016/j.seta.2019.02.008.
[41] Wang P, Wang K, Xi L, Gao R, Wang B. Fast and Accurate Performance Prediction and Optimization of Thermoelectric Generators with Deep Neural Networks. Adv Mater Technol 2021;6:1–8. https://doi.org/10.1002/admt.202100011.
[42] Wiecha PR, Arbouet A, Girard C, Muskens OL. Deep Learning in Nano-photonics: Inverse Design and Beyond. Photonics Res 2021;9:B182. https://doi.org/10.1364/prj.415960.
[43] Demeke W, Kim Y, Jung J, Chung J, Ryu B, Ryu S. Neural network-assisted optimization of segmented thermoelectric power generators using active learning based on a genetic optimization algorithm. Energy Reports 2022;8:6633–44. https://doi.org/10.1016/j.egyr.2022.04.065.
[44] Dinsdale NJ, Wiecha PR, Delaney M, Reynolds J, Ebert M, Zeimpekis I, et al. Deep Learning Enabled Design of Complex Transmission Matrices for Universal Optical Components. ACS Photonics 2021;8:283–95. https://doi.org/10.1021/acsphotonics.0c01481.
[45] Asano T, Noda S. Iterative Optimization of Photonic Crystal Nanocavity Designs by using Deep Neural Networks. Nanophotonics 2019;8:2243–56. https://doi.org/10.1515/nanoph-2019-0308.
[46] Fu L, Yin M, Wu D, Li W, Feng D, Huang L, et al. Large Enhancement of Thermoelectric Properties in N-type PbTe via Dual-site Point Defects. Energy Environ Sci 2017;10:2030–40. https://doi.org/10.1039/c7ee01871a.
[47] Zhang Q, Cao F, Liu W, Lukas K, Yu B, Chen S, et al. Heavy Doping and Band Engineering by Potassium to Improve the Thermoelectric Figure of Merit in P-type PbTe, PbSe, and PbTe1-ySey. J Am Chem Soc 2012;134:10031–8. https://doi.org/10.1021/ja301245b.
[48] Poudel B, Hao Q, Ma Y, Lan Y, Minnich A, Yu B, et al. High-thermoelectric Performance of Nanostructured Bismuth Antimony Telluride Bulk Alloys. Science (80-) 2008;320:634–8. https://doi.org/10.1126/science.1156446.
[49] Kosky P, Balmer R, Keat W, Wise G. Mechanical Engineering. Explor. Eng. 2013:259–81. https://doi.org/10.1016/B978-0-12-415891-7.00012-1.
[50] Shittu S, Li G, Zhao X, Ma X, Akhlaghi YG, Ayodele E. High Performance and Thermal Stress Analysis of a Segmented Annular Thermoelectric Generator. Energy Convers Manag 2019;184:180–93. https://doi.org/10.1016/j.enconman.2019.01.064.
[51] Kim HS, Kikuchi K, Itoh T, Iida T, Taya M. Design of segmented thermoelectric generator based on cost-effective and light-weight thermoelectric alloys. Mater Sci Eng B Solid-State Mater Adv Technol 2014;185:45–52. https://doi.org/10.1016/j.mseb.2014.02.005.
[52] Shen L, Zhang W, Liu G, Tu Z, Lu Q, Chen H, et al. Performance enhancement investigation of thermoelectric cooler with segmented configuration. Appl Therm Eng 2020;168:114852. https://doi.org/10.1016/j.applthermaleng.2019.114852.
[53] Ali H, Yilbas BS. Configuration of segmented leg for the enhanced performance of segmented thermoelectric generator. Int J Energy Res 2017;41:274–88. https://doi.org/10.1002/er.3620.
[54] Cai L, Li P, Luo Q, Zhai P, Zhang Q. Geometry Optimization of a Segmented Thermoelectric Generator Based on Multi-parameter and Nonlinear Optimization Method. J Electron Mater 2017;46:1552–66. https://doi.org/10.1007/s11664-016-5198-6.
[55] Chen WH, Bin Chiou Y. Geometry design for maximizing output power of segmented skutterudite thermoelectric generator by evolutionary computation. Appl Energy 2020;274:115296. https://doi.org/10.1016/j.apenergy.2020.115296.